Building an *in vivo* anatomical atlas to close the phenomic gap in animal breeding

Lars Erik Gangsei[a,c,*], Jørgen Kongsro[b], Kristin Olstad[d], Eli Grindflek[b], Solve Sæbø[c]

[a] *Animalia, P.O. Box 396 – Økern, N-0513 Oslo, Norway*
[b] *Norsvin SA, P.O. Box 504, N–2304 Hamar, Norway*
[c] *Norwegian University of Life Sciences, Department of Chemistry, Biotechnology and Food Science, Ås, P.O. Box 5003, N–1432 Ås, Norway*
[d] *Norwegian University of Life Sciences, Department of Companion Animal Clinical Sciences, Equine Section, Oslo, P.O. Box 8146 Dep, N–0033 Oslo, Norway*

Abstract

Currently, a growing gap is observed between the enormous amount of genomic information generated from genotyping and sequencing and the scale and quality of phenotypes in animal breeding. In order to fill this gap, new technologies and automated large-scale measurements are needed. Body composition is an important trait in animal breeding related to growth, feed efficiency, health, meat quality and market value of farmed animals. *In vivo* anatomical atlases from CT will aid large-scale and high-throughput phenotyping in order to reduce some of the gap between genotyping and phenotyping in animal breeding. We demonstrated that atlas segmentation was able to predict major parts and organs of the pig with a numerical test applied to the primal commercial cuts.

Keywords: Computed Tomography, pig, atlas, segmentation, breeding

1. Introduction

Recent advances in genome sequencing technology has led to high-throughput and high–density information in humans, animals and plants (Houle et al., 2010). Variation in phenotypes is produced through a web of interactions between genotype and environment, and there is a need for detailed phenotypic data to characterize the phenomes. Measuring body composition in farmed animal breeding is important in order to improve growth and feed efficiency, health,

*Corresponding author. Tel.: +47 95061231. E-mail address: lars.erik.gangsei@animalia.no

Email addresses: lars.erik.gangsei@animalia.no (Lars Erik Gangsei), jorgen.kongsro@norsvin.no (Jørgen Kongsro), kristin.olstad@nmbu.no (Kristin Olstad), eli.grindflek@norsvin.no (Eli Grindflek), solve.sabo@nmbu.no (Solve Sæbø)

meat quality and market value of carcasses (Nissen et al., 2006; Roche et al., 2009). Body composition has traditionally been assessed by a number of different means, ranging from subjective scoring (Fox & Black, 1984) or simple point measurements of subcutaneous fat (Silva et al., 2005) to physical dissection (Nissen et al., 2006) or chemical analysis (Shields et al., 1983) of carcasses or *in vivo* volume scans using Computed Tomography (CT) or Magnetic Resonance Imaging (MRI) (Szabo et al., 1999; Mitchell et al., 2001; Scholz et al., 2015).

For pigs, the use of CT makes it possible to obtain accurate *in vivo* measurements of body composition (Gjerlaug-Enger et al., 2012). Genetic selection on body composition traits in pigs was previously done by physical dissection of full-sibs and half-sibs of the selection candidates, which give much less accurate breeding value estimations compared with measuring body composition on the selection candidates themselves *in vivo*. Today, the pig breeding company Topigs Norsvin uses CT to measure body composition and monitor orthopedic disorders on 3.500 nucleus boars annually as an integrated part of their testing system. In this paper, we present an anatomical atlas from CT, which will help to close the phenomic gap in pig anatomy by giving access to high-throughput and high-dimensional anatomical phenotypes.

Obtaining *in vivo* body composition data from CT relies on segmentation of cross sectional slices. The segmentation strategies can be based on (1) intensities, applying adaptive thresholding of different tissues like adipose (fat), muscle and bone tissue (Skjervold et al., 1981), (2) shape or position using deformable models or active contours (McInerney & Terzopoulos, 1996), and (3) labelled atlas (Commowick, 2007). Methods are here ranked by complexity and demands of prior knowledge either from own data or literature. Automation of the segmentation methods would allow for detailed population studies of body composition. For atlas based segmentation, this paper shows how an atlas can be constructed using a subset of animals from the population of pigs.

The atlas can serve as a framework for building large data sets of anatomical phenotypes, paving the way to detailed and high–density phenotypic informa-

tion on pig anatomical traits. The number of additional variables in the breeding value estimation may be a limitation in terms of speed and complexity. The atlas phenotypes will be highly beneficial in terms of selection for animals with competitive advantages on muscle types, compared with the current selection in most breeding programs today, where results from CT are applied to muscle- and fat depth only (Gjerlaug-Enger et al., 2012). Creating atlases for primal cuts; "shoulder", "belly", "loin" and "ham", representing the market needs around the world would also make us able to sort our genetic material of pigs more efficiently in terms of different markets. Furthermore, by enhancing the anatomical traits by automatic segmentation, the accuracy of genetic selection for carcass traits will increase even further. The indirect effect of this is that more weight can be put in the breeding goal for hard-to-measure, low–heritable traits like maternal and disease-related traits, and in the end the whole breeding goal and genetic engine towards developing a more sustainable and accurate breeding program for farmed animals.

2. Methods

2.1. Approvement of the experiments

All animals were cared for according to laws, internationally recognized guidelines and regulations controlling experiments with live animals in Norway (Regulation for the keeping of pigs in Norway 2003-02-18-175 (in Norwegian), 2003; Animal welfare Act 2009-06-19-97 (in Norwegian), 2009); according to the rules given by Norwegian Animal Research Authority. The CT scans were also used in Gangsei & Kongsro (2016), which provides some more practical information about the scanning.

2.2. Data

The intensity atlas is in principle is the average of 386 nucleus boars, involving a total of approximately 3.4×10^{10} voxels (the 3D basic unit of the CT scans). The method was motivated by methods applied to micro CT scans of

mice (Baiker et al., 2010; Li et al., 2008), where the skeletons were utilized as a framework for conducting the transformations.

The raw CT scans were volume representations of the individual pigs. The size of 3D data arrays (volumes) were approximately $512 \times 512 \times 1200$, where the third dimension, size, varied slightly with pig length. Each data point represented a voxel with size 0.9355 mm $\times$0.9355 mm $\times$1.25 mm. A CT intensity according to the Hounsfield (HU) scale was associated with each voxel.

2.3. Atlas

The atlas represents the average pig. The atlas volume size was $500 \times 500 \times 1600$, where each voxel represents a cube with a side length of 1 mm. We use the expressions "intensity atlas" and "labelled atlas", where the intensities aligned to each voxel might be interpreted as HU–units. In the labelled version, every voxel is aligned to a specific label, i.e. organ, cut part etc.

Labelled and intensity volumes (3D) might be defined by a matrix representation, where the $N_y \times 3$ matrix $\mathbf{Y}$ and $N_x \times 3$ matrix $\mathbf{X}$, represent the atlas, and a random individual pig, respectively. N_y and N_x are the number of voxels in the respective images. Each row in $\mathbf{Y}$ and $\mathbf{X}$ defines the (Cartesian) coordinates for one voxel. The atlas was constructed through successive operations described in the next sections. Figures are used extensively to highlight important principles.

2.4. Skeleton atlas – image moments invariants

The first step was to identify the major bones in all pigs (Gangsei & Kongsro, 2016) (Fig. 1a). We calculated basic features for each bone, often referred to as image moments invariants (Hu, 1962): Center of mass (COM or $\bar{\mathbf{x}}$), the orthonormal basis of the bone ($\mathbf{R}$), volume ($v = n_\delta \times 0.9355^2 \times 1.25$, where n_δ is number of voxels) and length (l), that is, the Euclidian distance spanned by the bone along the first orthogonal basis vector. Left side bones were treated as right side bones by mirroring them over the sagittal plane before calculating the image moments invariants. The coordinates of each bone were represented

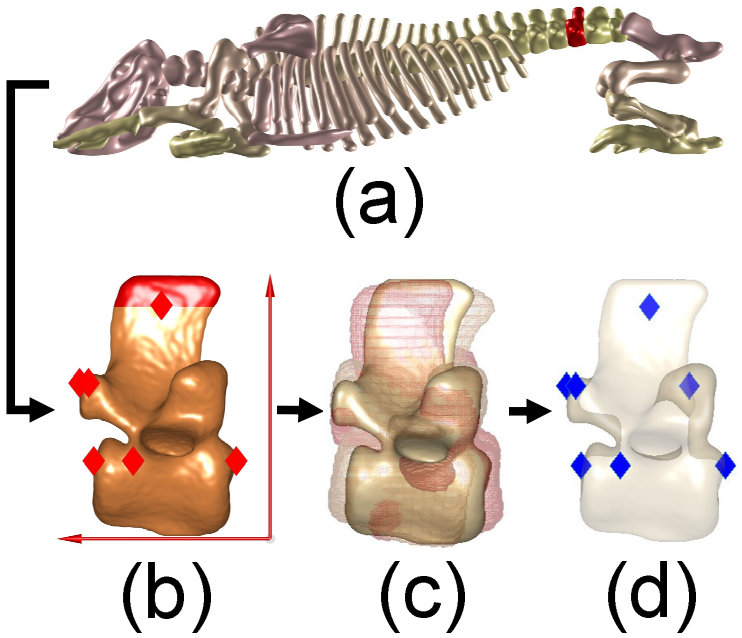

Figure 1: Construction of average bone by image moment invariants. (a) Segmented skeleton in a random pig; the vertebra illustrated in panels b–d is highlighted in red. (b) A vertebra with its orthonormal basis (arrows), landmarks, and the area where extra weight for orientation is added (red at top). (c) Construction of the average shape by rotating and scaling bones from all pigs to a common formwork. (d) Landmarks (blue) on the average vertebrae.

by the $n_\delta \times 3$ matrix $\mathbf{X}_\delta$. Furthermore, the diagonal weight matrix $\mathbf{W}$ assigned a specific weight to each voxel for the purpose of controlling the main directions of the orthonormal basis. The mathematical expressions for the COM and orthonormal basis were:

$$\bar{\mathbf{x}} = (1/n_\delta)\ \mathbf{X}_\delta^t \mathbf{1}_{n_\delta}, \quad \mathbf{R} = Eig\left\{\left(\mathbf{X}_\delta - \mathbf{1}_{n_\delta}\bar{\mathbf{x}}^t\right)^t \mathbf{W}^2 \left(\mathbf{X}_\delta - \mathbf{1}_{n_\delta}\bar{\mathbf{x}}^t\right)\right\}, \qquad (1)$$

where the notation $Eig\{\mathbf{A}\}$ denotes the eigenvectors of the matrix $\mathbf{A}$ scaled to unit length.

The concept of the weighting of voxels is shown in Fig. 1b, where the voxels in the red area, i.e. the voxels within a distance less than $1/10$ of the total length (l) from the top, were given heavy weights (100). Thus, the first column in $\mathbf{R}$,

i.e. the eigenvector having the largest corresponding eigenvalue, points approximately perpendicular to the coronal plane (upwards), the second eigenvector points approximately perpendicular to the transverse plane (forwards) and the third eigenvector points approximately perpendicular to the sagittal plane (to the left). For other bones, different parts were assigned additional weights, but the basic principle remains unchanged.

Based on the features of the individual bones we constructed atlas bones, i.e. templates for every bone in a pig (Fig. 1d). To every atlas bone, COM, volume, length, a common orthonormal basis and a shape, was applied. The COM ($\bar{\mathbf{x}}_T$), volume (v_T) and length (l_T) was just the average for all bones. For all bones in the spine and sternum, the COM value for the direction perpendicular to the sagittal plane (i.e. sideways), was set to 250 (mm). The common orthonormal basis, $\mathbf{R}_T$, was set to the individual orthonormal basis closest to the geometrically average ortonormal basis. Hence, by letting r_{ij} denote the element of the ith row and jth column of $\mathbf{R}$, and letting $\bar{r}_{ij}$ denote the average of the same element in all pigs, the $\mathbf{R}$ for which $\sum_{i=1}^{3}\sum_{j=1}^{3}\left(r_{ij}-\bar{r}_{ij}\right)^2$ had the minimum value was chosen as the common orthonormal basis for the bone in question.

In order to construct the average shape, all bones were transformed to a 3D image, $\mathbf{B}$, of predefined size, $m_1 \times m_2 \times m_3$, (Fig. 1c). The coordinates for the individual bones in these 3D images, denoted $\mathbf{Z}_\delta$, were given by rounded and scaled values of $(m_1/l)\ \mathbf{X}_\delta\mathbf{R}$. The scaling of $\mathbf{Z}_\delta$ was done by subtracting column means and adding column minimum values. Thus, every bone spanned the first dimension of $\mathbf{B}$ completely and was centred according to the two remaining dimensions. The final intensities of $\mathbf{B}$ equalled the sum of all bones transformed into it. The average shape was constructed by setting a threshold making sure that the volume of voxels in $\mathbf{B}$ having higher intensity than this threshold, was equal to the average volume of the bone (v_T).

2.5. Corresponding landmarks

The crucial steps of the method involved constructing corresponding landmarks between the volumes of the individual pigs (Fig. 2a–c). The initial step (Fig. 1d), was to set landmarks at approximately every 20mm along the main direction of the orthonormal basis of the average shaped bone. The landmarks were set either at the top, bottom, right and left side of the surface or in the centre of the bone (typically for ribs, hand and foot). In total approximately 1200 landmarks on the skeleton were identified (Fig.2a), varying with the number of vertebras and ribs in the individual pigs. The coordinates of the landmarks in the common orthogonal basis, $\mathbf{R}_T$, are denoted $\mathbf{Z}_l$, and the corresponding COM is denoted $\bar{\mathbf{z}}$.

These landmarks were transformed back to the basis of the individual pigs and the atlas by reversing the transformations based on image moments invariants. The common averages were used for the transformation to the atlas space resulting in a pattern symmetric over the sagittal plane (Fig. 2b). Individual image moments invariants were used for the individual pigs; consequently there was no symmetric pattern for these points (Fig. 2a). The mathematical expressions for the reverse transformations are given by:

$$\begin{aligned} \mathbf{Y}_l &= (l_T/m_1)\ (\mathbf{Z}_l - \mathbf{1}_{n_l}\bar{\mathbf{z}})\,\mathbf{R}_T^{-1} + \mathbf{1}_{n_l}\bar{\mathbf{x}}_T \\ \mathbf{X}_l &= (l_T/m_1)\ (v/v_T)^{1/3}\ (\mathbf{Z}_l - \mathbf{1}_{n_l}\bar{\mathbf{z}})\,\mathbf{R}^{-1} + \mathbf{1}_{n_l}\bar{\mathbf{x}} \end{aligned} \tag{2}$$

, where the landmarks in the atlas and individual pigs are denoted $\mathbf{Y}_l$ and $\mathbf{X}_l$, respectively.

2.6. Non–rigid transformation

The stacked matrices of $\mathbf{Y}_l$–s and $\mathbf{X}_l$–s (all bones), are denoted $\mathbf{Y}_1$ and $\mathbf{X}_1$. These matrices were used to construct a cubic B-spline based transformation of $\mathbf{X}_1$ to $\mathbf{Y}_1$. The underlying model for the transformation is:

$$\mathbf{Y}_1 = \mathbf{Q}_{1X}\beta_1 + \mathbf{E}_1, \tag{3}$$

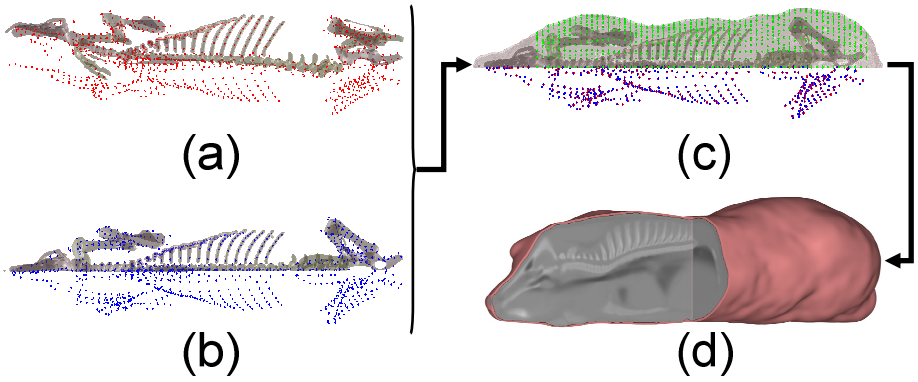

Figure 2: Construction of corresponding landmarks and the intensity atlas. (a) Landmarks for all bones transformed back to the original space of the pig. (b) Landmarks of all average bones transformed to the atlas space. (c) Non–rigid transformation based on the skeleton landmarks applied to the skeleton (blue/ red) and surface (skin). A secondary set of landmarks on the pig surfaces (green). (d) The intensity atlas. I.e. average HU–units after all voxels of all pigs are transformed to the atlas space.

, where $\mathbf{Q}_{1X}$ denotes a matrix of size $n_1 \times p_L$ the elements of which were calculated by tensor (cubic) B-spline functions using $\mathbf{X}_1$ as input. The parameter β_1 denotes the regression parameters and $\mathbf{E}_1$ random noise. We utilized existing software (Kroon, 2011a,b) for the implementation of all B-spline based transformations. The software automatically calculated $\mathbf{Q}_{1X}$ including optimizing the knot grid used in the cubic B-spline functions, and provided estimates, $\hat{\beta}_1$, of β_1 for all pigs based on the input $\mathbf{X}_1$ and $\mathbf{Y}_1$.

For all pigs the surface voxels (skin) were identified, with coordinates denoted $\mathbf{X}_S$. The surface points from all 386 pigs were transformed to a common 3D image, $\mathbf{S}$, with the same dimensions as the atlas, by applying the transformation based on skeleton landmarks. The mathematical formula for this transformation is written as $\hat{\mathbf{Y}}_S = \mathbf{Q}_{SX}\hat{\beta}_1$ where the rounded values of $\hat{\mathbf{Y}}_S$ gave the coordinates of the surface voxels $\mathbf{X}_S$ transformed to $\mathbf{S}$. In order to get a symmetric surface, $\mathbf{S}$ was mirrored over the sagittal plane. The final atlas surface was defined as the voxels in $\mathbf{S}$ having maximum intensity and composing a continuous, connected surface.

For every 20 mm, on the interval from 200mm to 1400mm, along the longitudinal axis of the atlas surface, 34 new landmarks were set on the average surface (Fig. 2c). These points were set at a fixed set of angles around the centre of the slice in question. The coordinates of these landmarks are denoted $\mathbf{Y}_2$. Corresponding points for individual pigs, $\mathbf{X}_2$, were set as the surface points in $\mathbf{X}_S$ of which the corresponding transformed points, i.e. $\hat{\mathbf{Y}}_S$, had the minimum Euclidian distance to the points in $\mathbf{Y}_2$.

The motivation for constructing the corresponding points on the surface, i.e. $\mathbf{Y}_2$ and $\mathbf{X}_2$, was to increase the precision of the final B-spline transformations that were applied to the full volumes of the original pigs. Hence, the coordinates of the full volumes were the rounded values of $\hat{\mathbf{Y}} = \mathbf{Q}_{12X}\hat{\beta}_{12}$, where the basic functions of $\mathbf{Q}_{12X}$ and $\hat{\beta}_{12}$ were calculated using the stacked matrices of $\mathbf{Y}_1$ and $\mathbf{Y}_2$, and $\mathbf{X}_1$ and $\mathbf{X}_2$. The final intensity–based result is illustrated in Fig. 2d. The intensities of the voxels in the intensity atlas are simply the average HU-unit after the final transformation of all voxels in all pigs.

2.7. Labelled atlas – atlas segmentation

A labelled version of the atlas (Fig. 3a–b), was constructed by manual segmentation of the intensity atlas. The final step was to transform the labels onto the individual pigs, or eventually, onto new pigs registered to the atlas. Since every voxel in the individuals transformed to the (labelled) atlas corresponds to exactly one voxel in the atlas, the label of all voxels in individual pigs are easily defined (Fig. 4a–d).

The inner organs were segmented out by methods combining thresholds (HU-units) in the intensity atlas, and manual segmentation. The commercial cuts were set by segmenting the shoulder, which also includes the head, from loin and belly by a cut exactly in the transverse plane of the atlas. The ham and loin were also segmented by a cut in the transverse plane. Belly was segmented from ham and loin by manual segmentation based on the intensity atlas.

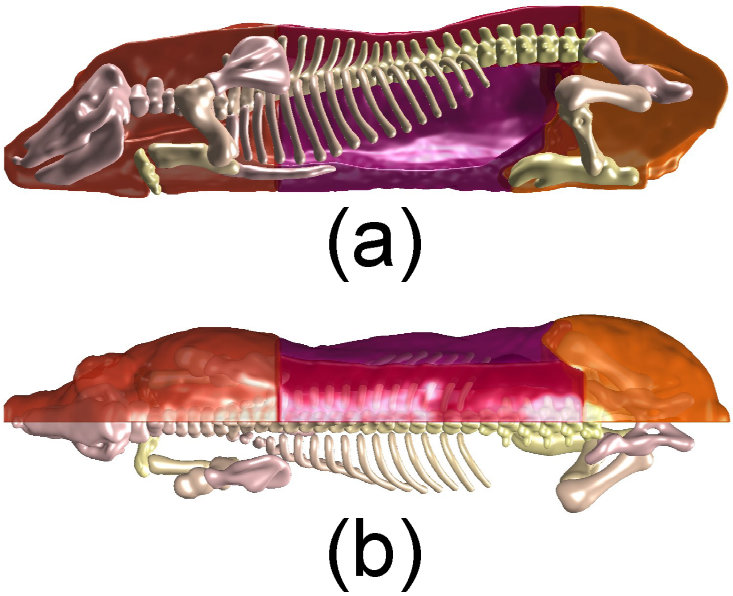

Figure 3: The labelled atlas. (a) View perpendicular to the sagittal plane. (b) View perpendicular to the coronal plane. In both panels ham is shown with orange color, belly with violet color, loin with clear red color and shoulder with red/ brown color. The major bones in the skeleton are shown withe different shades in gray/ yellow/ pink colors.

2.8. Validation

First and foremost the method was validated by visual inspection of the segmentation applied to the individual pigs.

In order to conduct a numerical test of the method, we applied atlas segmentation to the primal cuts of 52 headless carcasses (left half) (Fig. 4). We predicted the weights of all voxels by applying a simple regression equation for voxel density (kg/m^3) using the intensities, measured as Hounsfield units (HU), as predictor variable. The regression parameters were calculated by ordinary least squares regression using the registered weights of all 52 carcasses as response.

The corresponding cut weights (kg) and their proportions (% of carcass weight) (carcass right half) were registered by butchers at the Norwegian Meat and Poultry Research Center (Animalia) pilot plant. Thus we were able to cal-

culate the correlations between cut weights and cut proportions based on two independent methods, i.e. atlas segmentation and manual butchering. Variances in cut proportions are, unlike variances in the cut weights, independent of total carcass weight. Thus, an eventual significant positive correlation for cut proportions, as opposed to the correlation between cut weights, might be viewed as a strong indication of the validity of the atlas segmentation method.

2.9. Code availability

All computations were conducted using the software MATLAB (MATLAB, 2015). A demonstration of the central parts of the computer code applied to data from parts of a random pig is included as supplementary material in the zipped folder "Code_and_Data.zip".

3. Results

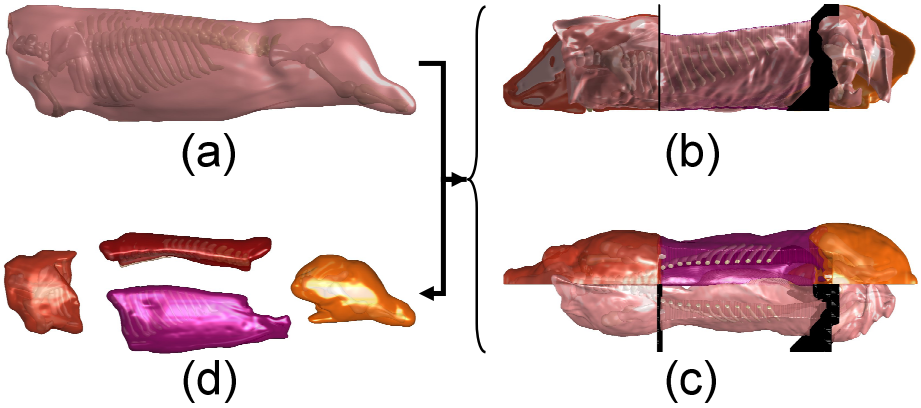

Figure 4: Atlas segmentation applied to a carcass (left half). (a) An untransformed carcass. (b–c) The carcass (left hand side) registered (transformed) to the atlas (right hand side). The loin cut is removed to increase visibility. The other cuts are illustrated as black surfaces. (d) The final segmentation for the carcass in its four major cuts.

Visual inspection of the individual carcasses after transformation show that the method has an acceptable accuracy for atlas segmentation of the major parts, for an example see supplementary Video 1. The accuracy is best close

to the skeleton structure, where the density of landmark is huge, whereas the accuracy declines in areas where landmarks are scarce, typically in the back part of the belly.

The correlations between cut weight measured by atlas segmentation and manual butchering were 0.95, 0.91, 0.87 and 0.95 for shoulder-, belly-, loin- and ham weights, respectively. For the cut proportions the corresponding correlations were 0.60, 0.38, 0.36 and 0.47, all significantly different from 0 ($p < 0.01$). The variation in cut proportions between individuals were small, i.e. standard deviation at approximately 1 % unit.

4. Discussion

Differences in predicted cut weights between left and right sides might be substantial due to morphological differences, butcher effects and inaccurate splitting of carcasses. For shoulder and belly weights, differences between butchers are reported as high as 6–10% (Nissen et al., 2006). Thus, the correlation between the cut weights registered by butchers and by atlas segmentation was not expected to be extremely high even with a perfect atlas segmentation. For the cut proportions the *a priori* expected correlation between the two methods were substantially lower, due to the small variation in cut proportions between individuals. Thus, the highly significant positive correlations is a strong support for the usefulness of atlas segmentation.

The transformations were solely based on corresponding landmarks. The state–of–the–art methods in medical image analysis, see Sotiras et al. (2013) for an overview, would generally include an extra step involving fine tuning of the transformation based on image intensities, typically based on the Gauss–Newton algorithm (Gill & Murray, 1978). This step aims at minimizing the cost based on a similarity measure between individual pigs and the intensity atlas (reference and template), utilizing the intensities of all data points. The transformations and intensity atlas described in this paper would constitute a natural starting point for such an algorithm. If successful, the result would be

an even finer tuned intensity atlas, which in turn enables construction of a more detailed labelled atlas. However, there is a substantial risk associated with such methods as they may result in convergence to local optima, or yield over–fitted solutions, i.e. applying too much non-rigid deformation.

The full set of landmarks is the joint set of the original skeleton–landmarks and the surface–landmarks. The surface–landmarks are set based on a provisional transformation of the full surface, based on the skeleton–landmarks. We applied a simple method based on euclidian distances to define the surface landmarks. As part of our further work we would like to evaluate 3D point matching algorithms (Tam et al., 2013) as an alternative for defining these landmarks. We would also like to evaluate the possibility for identifying more landmarks prior to the final transformation. In particular landmarks defining the surface separating the internal organs from the commercial cuts would have been valuable.

For a whole-body analysis, the corresponding landmarks are sufficient to obtain a satisfactory level of accuracy. As the method is automatic and robust, it offers a potential of multiplying the level of registered phenotypic variation for the full parental lines of breeding pigs. Thus it might constitute the foundation for the next generation of high-throughput and high-density phenotyping in animal breeding.

5. Acknowledgements

Lars Erik Gangsei was supported by the Research Council of Norway, grant 225294 (PigComp).

6. References

Animal welfare Act 2009-06-19-97 (in Norwegian) (2009). Lov om dyrevelferd. Lovdata. URL: `https://lovdata.no/dokument/NL/lov/2009-06-19-97` (Accessed: 19th February 2016).

Baiker, M., Milles, J., Dijkstra, J., Henning, T. D., Weber, A. W., Que, I., Kaijzel, E. L., Löwik, C. W., Reiber, J. H., & Lelieveldt, B. P. (2010). Atlas-

based whole–body segmentation of mice from low–contrast Micro–CT data. *Medical Image Analysis*, *14*, 723–737. doi:10.1016/j.media.2010.04.008.

Commowick, O. (2007). *Design and Use of Anatomical Atlases for Conformal Radiotherapy Planning*. Ph.D. thesis INRIA Sophia Antipolis, France.

Fox, D., & Black, J. (1984). A system for Predicting Body Composition and Performance of Growing Cattle. *Journal of Animal Science*, *58*, 725–739. doi:doi:10.2134/jas1984.583725x.

Gangsei, L. E., & Kongsro, J. (2016). Automatic segmentation of Computed Tomography (CT) images of domestic pig skeleton using a 3D expansion of Dijkstras algorithm. *Computers and Electronics in Agriculture*, *121*, 191–194. doi:10.1016/j.compag.2015.12.002.

Gill, P. E., & Murray, W. (1978). Algorithms for the Solution of the Nonlinear Least-Squares Problem. *SIAM Journal on Numerical Analysis*, *15*, 977–992. doi:10.1137/0715063.

Gjerlaug-Enger, E., Kongsro, J., Odegård, J., Aass, L., & Vangen, O. (2012). Genetic parameters between slaughter pig efficiency and growth rate of different body tissues estimated by computed tomography in live boars of Landrace and Duroc. *Animal*, *6*, 9–18. doi:10.1017/S1751731111001455.

Houle, D., Govindaraju, D. R., & Omholt, S. (2010). Phenomics: the next challenge. *Nature Reviews Genetics*, *11*, 855–66. doi:10.1038/nrg2897.

Hu, M.-K. (1962). Visual pattern recognition by moment invariants. *Information Theory, IRE Transactions on*, *8*, 179–187. doi:10.1109/TIT.1962.1057692.

Kroon, D.-J. (2011a). B-spline grid, image and point based registration. MATLAB Central File Exchange. (c) 2009; Dirk–Jan Kroon. Retrieved June 02, 2015.

Kroon, D.-J. (2011b). *Segmentation of the Mandibular Canal in Cone-beam CT Data*. Ph.D. thesis University of Twente, Enschede, The Netherlands.

Li, X., Yankeelov, T. E., Peterson, T. E., Gore, J. C., & Dawant, B. M. (2008). Automatic nonrigid registration of whole body CT mice images. *Medical Physics*, *35*, 1507–1520. doi:10.1118/1.2889758.

MATLAB (2015). *Version 8.5.0 (R2015a)*. Natick, Massachusetts: The MathWorks Inc.

McInerney, T., & Terzopoulos, D. (1996). Deformable models in medical image analysis: a survey. *Medical Image Analysis*, *1*, 91–108. doi:10.1016/S1361-8415(96)80007-7.

Mitchell, A., Scholz, A., Wange, P., & Song, H. (2001). Body composition analysis of the pig by magnetic resonance imaging. *Journal of Animal Science*, *79*, 1800–1813. doi:doi:/2001.7971800x.

Nissen, P. M., Busk, H., Oksama, M., Seynaeve, M., Gispert, M., Walstra, P., Hansson, I., & Olsen, E. (2006). The estimated accuracy of the EU reference dissection method for pig carcass classification. *Meat Science*, *73*, 22–28. doi:10.1016/j.meatsci.2005.10.009.

Regulation for the keeping of pigs in Norway 2003-02-18-175 (in Norwegian) (2003). For 2003-02-18 nr 175: Forskrift om hold av svin. Lovdata. URL: https://lovdata.no/dokument/SF/forskrift/2003-02-18-175 (Accessed: 19th February 2016).

Roche, J. R., Friggens, N. C., Kay, J. K., Fisher, M. W., Stafford, K. J., & Berry, D. P. (2009). Invited review: Body condition score and its association with dairy cow productivity, health, and welfare. *Journal of Dairy Science*, *92*, 5769–5801. doi:10.3168/jds.2009-2431.

Scholz, A., Bünger, L., Kongsro, J., Baulain, U., & Mitchell, A. (2015). Non–invasive methods for the determination of body and carcass composition in livestock: dual-energy X–ray absorptiometry, computed tomography, magnetic resonance imaging and ultrasound: invited review. *Animal*, (pp. 1–15). doi:10.1017/S1751731115000336.

Shields, R., Mahan, D., & Graham, P. (1983). Changes in Swine Body Composition from Birth to 145 Kg. *Journal of Animal Science*, *57*, 43–54. doi:10.2134/jas1983.57143x.

Silva, S., Gomes, M., Dias-da Silva, A., Gil, L., & Azevedo, J. M. T. d. (2005). Estimation in vivo of the body and carcass chemical composition of growing lambs by real–time ultrasonography. *Journal of Animal Science*, *83*, 350–357. doi:doi:/2005.832350x.

Skjervold, H., Grønseth, K., Vangen, O., & Evensen, A. (1981). In vivo estimation of body composition by computerized tomography. *Zeitschrift für Tierzüchtung und Züchtungsbiologie*, *98*, 77–79. doi:10.1111/j.1439-0388.1981.tb00330.x.

Sotiras, A., Davatzikos, C., & Paragios, N. (2013). Deformable Medical Image Registration: A Survey. *IEEE transactions on medical imaging*, *32*, 1153–1190. doi:10.1109/TMI.2013.2265603.

Szabo, C., Babinszky, L., Verstegen, M., Vangen, O., Jansman, A., & Kanis, E. (1999). The application of digital imaging techniques in the in vivo estimation of the body composition of pigs: a review. *Livestock Production Science*, *60*, 1–11. doi:10.1016/S0301-6226(99)00050-0.

Tam, G. K., Cheng, Z.-Q., Lai, Y.-K., Langbein, F. C., Liu, Y., Marshall, D., Martin, R. R., Sun, X.-F., & Rosin, P. L. (2013). Registration of 3D Point Clouds and Meshes: A Survey from Rigid to Nonrigid. *IEEE transactions on visualization and computer graphics*, *19*, 1199–1217. doi:10.1109/TVCG.2012.310.